ACS NANO
Cite This: ACS Nano 2018, 12, 5719–5725
www.acsnano.org

ARTICLE

Reflectivity Effects on Pump–Probe Spectra of Lead Halide Perovskites: Comparing Thin Films *versus* Nanocrystals

Tufan Ghosh, Sigalit Aharon, Adva Shpatz, Lioz Etgar, and Sanford Ruhman*

Institute of Chemistry, The Hebrew University of Jerusalem, Jerusalem 9190401, Israel

Supporting Information

ABSTRACT: Due to the sizable refractive index of lead halide perovskites, reflectivity off their interface with air exceeds 15%. This has prompted a number of investigations into the prominence of photoreflective contributions to pump–probe data in these materials, with conflicting results. Here we report experiments aimed at assessing this by comparing transient transmission from lead halide perovskite films and weakly quantum confined nanocrystals of cesium lead iodide ($CsPbI_3$) perovskite. By analyzing how complex refractive index changes impact the two experiments, results demonstrate that changes in absorption and not reflection dominate transient transmission measurements in thin films of these materials. None of the characteristic spectral signatures reported in such experiments are exclusively due to or even strongly affected by changes in sample reflectivity. This finding is upheld by another experiment where a methyl ammonium lead iodide ($MAPbI_3$) perovskite film was formed on high-index flint glass and probed after pump irradiation from either face of the sample. We conclude that interpretations of ultrafast pump–probe experiments on thin perovskite films in terms of photoinduced changes in absorption alone are qualitatively sound, requiring relatively minor adjustments to factor in photoreflective effects.

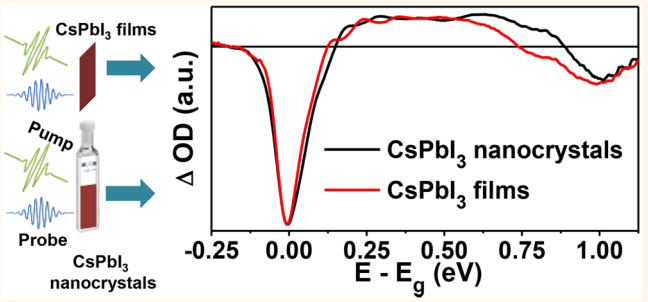

KEYWORDS: *lead halide perovskite, perovskite nanocrystals, absorption and reflectivity of perovskites, photoinduced refractive index change, ultrafast spectroscopy*

The high-energy conversion efficiency obtained in solar cells based on lead halide perovskites (LHP) has been attributed to their intense absorption, long carrier diffusion length, and slow electron–hole recombination rates.[1−7] Much recent research has been concentrated on figuring out how these structurally inhomogeneous and seemingly defect laden thin semiconducting films nonetheless attain this performance.[8−12] As part of this effort, exciton and free carrier dynamics have been followed using ultrafast spectroscopy on various perovskite materials, ranging from bulk thin films to single crystals of various dimensions, and differing in composition from all inorganic to hybrid perovskites where alkyl-ammonium groups replace alkali metal cations.[13−26]

Following a brief phase of exciton dissociation, recently observed with extreme time-resolution pump–probe experiments,[25] a number of common spectral features have been reported in numerous transient transmission (TT) studies of $MAPbI_3$ thin films (use of this abbreviation and not TA (transient absorption) will be explained shortly).[13,15,18,20,21,26] First is a rapid build-up of intense photoinduced bleach (PIB), positioned at the band gap (BG), which further grows to its full intensity during the subsequent carrier cooling. An analogous but weaker bleach concurrently appears surrounding a higher absorption peak near 480 nm.[25,26] Second is an equally rapid appearance of a short-lived photoinduced absorption (PIA) below the BG which decays on picosecond timescales presumably due to carrier cooling. Third is a broad and shallow PIA above the BG which develops gradually during carrier cooling, spanning the range from 550 to 680 nm.

The PIB at the band edge (BE) is often assigned to state filling and hot carrier-induced screening of the exciton transition.[13,18] The short-lived PIA below the BE is attributed to BG renormalization in presence of hot carriers.[18,20] However, assignment of the broad PIA which rises in the mid-visible remains controversial. Deschler and co-workers simultaneously measured transient reflectivity and transmission from photoexcited $MAPbI_3$ films, concluding that the broad and long-lived reduced transmission in the visible is primarily

Received: February 28, 2018
Accepted: May 4, 2018
Published: May 4, 2018

DOI: 10.1021/acsnano.8b01570
ACS Nano 2018, 12, 5719–5725

due to enhanced reflectivity and not to a boost in absorption.[27] Beard and co-workers have also addressed the contribution of reflectivity to the transient optical response in $MAPbI_3$ films.[20,28] Contrary to the Deschler group, they maintain that BG renormalization is the primary source of this apparent absorption. This view has been seconded by Anand *et al.*,[26] who, aside from extending their spectral coverage of transmission changes deeper in the UV, have shown that photorefractive-induced reflectivity changes should be too small to explain the appearance of this broad absorption feature.

While controversy has focused on this particular band, it highlights a general difficulty in interpreting transient transmission data from polycrystalline thin films. In typical pump–probe experiments, it is the sample transmission which is recorded, being the sum of photoinduced changes both in absorption and reflection. In many investigated samples, such as dilute solutions of molecular chromophores, changes in reflectivity are irrelevant and transmission can be assigned to variations in absorption alone. In inorganic semiconductors as in LHP samples, the refractive index in the visible is much higher than that of vacuum or of transparent glasses,[29,30] and thus both effects need to be assessed separately before pump–probe data for such samples can be interpreted in terms of the underlying physical mechanisms.[31]

Simultaneous measurement of transient reflectivity is the obvious path for assessing its contribution to transient transmission. But as described above, this approach has been tried by several groups with conflicting results.[20,27] Deposition of polycrystalline LHP films by wet chemical processing leads to rough scattering interfaces, measuring reflectivity from which is experimentally challenging. It is thus desirable to augment this method with other experimental approaches. Here we report the results of two experiments addressing this issue. In the first, pump–probe data from $CsPbI_3$ nanocrystals is compared with measurements from thin films of the same material. The second compares transient transmission changes in $MAPbI_3$ thin films deposited on high-index flint glass substrates after pumping from either face of the sample. Results of both experiments demonstrate that reflectivity changes do not make dominant contributions to TT spectra of LHP thin films anywhere in the visible to NIR, including in the broad PIA which motivated this study. Thus the debated long-lived reduced transmission band which rises on the ps time scale in the mid-visible must result chiefly from enhanced absorption in the perovskite.

RESULTS AND DISCUSSION

Experimental Design. The rationale behind these experiments is to compare TT measurements on different LHP samples where the relative contributions of reflectivity and absorbance, or more precisely of changes in the real and imaginary components of the refractive index, are very different. As recognized early on in the study of nanocrystals, Rayleigh scattering cross sections fall so steeply with particle size ($\sim r^6$), that colloidal nanocrystals whose diameter is a small fraction of the wavelength essentially do not scatter.[32,33] Often such miniaturization is accompanied with significant changes to their spectroscopy and photodynamics due to quantum confinement.[34,35] In the case of LHPs, moderate exciton Bohr radii allow for synthesis of weakly confined nanocrystals which on the one hand emulate the bulk in terms their photoresponse,[23] but at the same time do not scatter.

The absorption cross section of a nanocrystal of volume v in terms of its complex refractive index $\tilde{n} = n + i\kappa$ and that of its (non-absorbing) surroundings n_0 is:[32]

$$\begin{cases} \sigma_{abs}(\omega) = \dfrac{2\omega}{n_0 c} |f_\omega|^2 \, n\kappa v \\ f_\omega = \dfrac{3n_0^2}{(2n_0^2 + \tilde{n}^2)} \end{cases} \quad (1)$$

where f_ω is a local field factor which must be included since it depends on the same refractive indices. For a polycrystalline film or a crystal, reflectivity at the interface with a non-absorbing dielectric, whose refractive index is n_0, is given by the Fresnel relation (eq 2):

$$R = (\tilde{n} - n_0)^2/(\tilde{n} + n_0)^2 = [(n - n_0)^2 + \kappa^2]/[(n + n_0)^2 + \kappa^2] \quad (2)$$

The first derivatives of σ_{abs} or of R (both of which reduce transmission) with respect to n or κ quantify their sensitivity to variations in either constant. Table 1 presents values for these derivatives at a few relevant wavelengths, both for nanocrystal absorption and for film reflectivity at interfaces with air, fused silica, and NSF6 flint glass. $CsPbI_3$ is used in the nanocrystal experiments instead of the more studied $MAPbI_3$ since they share very similar spectroscopy and dynamics (Figure 1), but cesium-based nanocrystals are far more stable.[36] Since thin films of $CsPbI_3$ are unstable in contact with air, encapsulation was necessary for comparison with crystallites. Numerous studies have shown close similarities in the transient and linear optical properties for both, in particular both have nearly identical κ and exhibit the same rising mid-visible PIA which is the focus here.[23−25,37] For this reason, pump–probe data of nanocrystals are compared here with $CsPbI_3$ thin film results where both pump and probe impinge on the sample through a fused silica substrate. In accordance with the literature, we use the same optical constants to analyze the data for both materials.[37] The bottom panel of Figure 1 demonstrates the close resemblance of the absorption spectra of both perovskites,

Table 1. Values of First Derivative of Reflectivity (R) and the Ratio of Those for Nanocrystal Absorption Cross Section (σ) with Respect to n and κ[a]

Interface/ medium	$MAPbI_3$ or $CsPbI_3$ films					
	dR/dn			$dR/d\kappa$		
	E_g+0.6 eV	E_g+0.26 eV	E_g	E_g+0.6 eV	E_g+0.26 eV	E_g
Air/LHP	0.12	0.13	0.13	0.05	0.03	0.02
Quartz/LHP	0.09	0.09	0.09	0.04	0.02	0.02
NSF6/LHP	0.06	0.06	0.06	0.04	0.02	0.02
Hexane	$CsPbI_3$ nanocrystals					
	$\frac{d\sigma/dn}{d\sigma/d\kappa}$					
	E_g+0.6 eV		E_g+0.26 eV		E_g	
	-0.26		-0.12		-0.08	

[a]The refractive index of NSF6: 1.8, quartz: 1.46, and hexane: 1.37 has been used for the calculation. The values of refractive index of LHP at different wavelengths were adopted from ref 29.

DOI: 10.1021/acsnano.8b01570
ACS Nano 2018, 12, 5719–5725

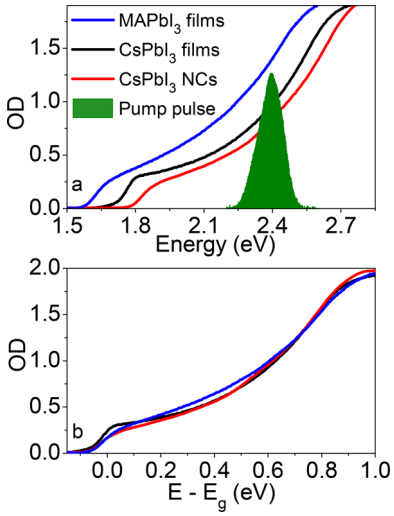

Figure 1. Transmission spectra of $MAPbI_3$ and $CsPbI_3$ films plus with that of hexane dispersed nanocrystals of the latter. (a) (Plus pump spectrum) shows similarity aside from shifts in absorption edges (1.65, 1.8, and 1.85 eV for $MAPbI_3$ films, $CsPbI_3$ films, and $CsPbI_3$ nanocrystals, respectively). (b) Same spectra on an energy scale shifted by the BG of each.

including the large nanocrystal sample, once plotted on an energy scale shifted by the BG.

Table 1 reveals how both a change in the substrate index as well as going from thin film to nanocrystal samples changes the ratio of first derivatives with respect to n and κ. In the case of nanocrystals not only does the absolute value

$$\left|\frac{d\sigma/dn}{d\sigma/d\kappa}\right|$$

change relative to

$$\left|\frac{dR/dn}{dR/d\kappa}\right|$$

of a thin film, the ratio itself changes sign. If the PIA band at ~600 nm is only due to induced reflectivity in thin films, then it reflects changes in n and not κ since the latter would also impact absorbance. There is however no argument that transmission changes near the BE of perovskite thin films are strongly affected by changes in κ. Adding all this up indicates that if Deschler and co-workers assignment of the broad PIA is correct,[27] then the signals in the nanocrystals and in thin films should be drastically different, transforming the mid-visible band from an apparent PIA into a bleach!

These arguments explain the incentive for comparison between thin films and nanocrystals. The derivatives in Table 1 also present the opportunity for another experiment to test the same issue in $MAPbI_3$ thin films. Just changing from an air/LHP to NSF6/LHP interface already changes

$$\left|\frac{dR/dn}{dR/d\kappa}\right|$$

by a factor of nearly 2 in the mid-visible. Exciting a thin film of $MAPbI_3$ which is a few hundred nanometers thick, with a pump centered at 520 nm, leads to an uneven depth distribution of excited carriers. As shown by Yang *et al.*,[28] this exponentially diminishing concentration profile will equilibrate spatially only over tens of picoseconds. Thus in the same sample, concentrating excitation on either face of the sample will change the relative significance of Δn and $\Delta\kappa$ to the reflectivity, explaining the impetus for the second series of measurements. The selection of whether the pump impinges on the air/LHP or NSF6/LHP face of the sample can achieve this variation without significant deterioration of time resolution, given the shallow depth of the sample (~200 nm).

Femtosecond Transient Transmission Measurements. Figure 2 presents transient transmission data from $CsPbI_3$ films

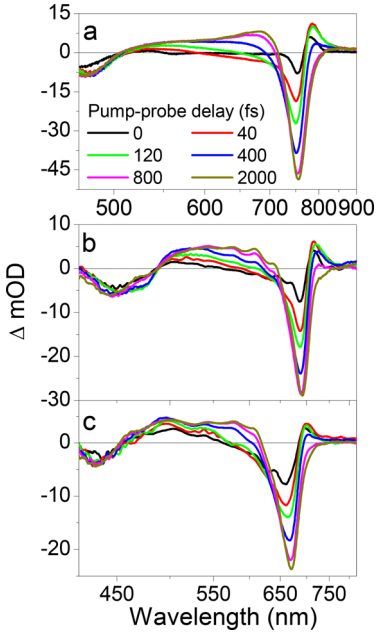

Figure 2. Transient difference transmission spectra of (a) $MAPbI_3$ films, (b) $CsPbI_3$ films, and (c) $CsPbI_3$ nanocrystals after excitation with 520 nm pulses. The pump−probe delays are shown in the inset.

and nanocrystals together with analogous data from a thin film of hybrid $MAPbI_3$ perovskite. All three data sets exhibit a similarly evolving series of common spectral features. Immediately after photoexcitation, a short-lived narrow band appears to the "red" of the optical BE, assigned to the hot carrier-induced BG renormalization and shifting of the excitonic transition. At the same time, a partial PIB appears at the optical BG due to state filling compounded with reduced coulomb enhancement of the exciton transition through carrier-induced screening. This bleach grows to its full intensity during the carrier cooling within ~1.5 ps as shown explicitly in Figure 3. A broad absorption appears to the "blue" of the BG which further broadens during the carrier cooling. Even further to the blue, a bleach and shift feature is apparent in all three samples. It builds up immediately, but unlike the BE bleach it does not exhibit spectral changes during carrier cooling. The main difference between the two cesium samples relative to the $MAPbI_3$ films is a shift of the BG to the blue. Additional wave-like modulations of the TT spectra particular to the $CsPbI_3$ samples at all pump−probe delays are related to residual phase ripples from the matched chirped mirrors used to compress the broad supercontinuum probe pulses, and these modulations have nothing to do with optical changes of the sample. Similar ripples are not seen in case of TT spectra of $MAPbI_3$ (Figure 2a) since these spectra were recorded in a set up without probe compression using these mirrors.

DOI: 10.1021/acsnano.8b01570
ACS Nano 2018, 12, 5719−5725

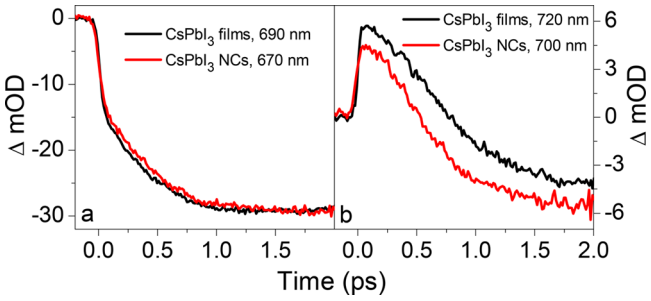

Figure 3. Temporal changes at the (a) BE bleach and (b) below BE PIA during carrier cooling in $CsPbI_3$ perovskite films (black) and nanocrystals (red) after 520 nm excitation. The data for nanocrystals are normalized according to the bleach intensity in the films for both the graphs.

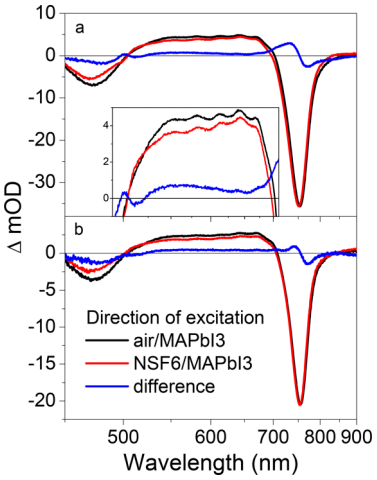

Figure 4. Transient difference transmission spectra of $MAPbI_3$ films at 3 ps after excitation with 520 nm pulses with two different pump fluences (a) 35 $\mu J/cm^2$ and (b) 25 $\mu J/cm^2$. The probe was sent from the air/perovskite interface while the pump beam was sent either from air/perovskite interface (black) or high index glass/perovskite interface (red). The blue line represents the spectral difference between the air/perovskite and high index glass/perovskite spectra. Inset in top panel shows enlarged view of broad PIA band with same axis labels as Figure 4a.

Figure 2b,c show that transient spectra recorded for $CsPbI_3$ in the form of nanocrystals and a thin film are surprisingly similar. The debated below BG induced absorption is apparent in both samples with nearly identical intensity. When relating to intensity, we refer to the intensity of the induced absorption relative to that of the exciton bleaching signals at ∼700 nm. As discussed below, this similarity serves to demonstrate that the PIA under study is primarily due to variations in sample absorption related to κ the imaginary part of the sample index. This similarity applies not only to spectral profiles but also to decay kinetics. Figure 3 shows temporal cuts at representative wavelengths from TT data of $CsPbI_3$ films and nanocrystals. The BE bleach is composed of an instantaneous jump (∼50% of total bleach) followed by a relatively slow decaying component with a lifetime, $\tau \sim 0.4$ ps, assigned to carrier cooling. Figure 3a,b compares BE bleach build up and below BG PIA decays in nanocrystals and in the thin films, respectively. These two features also show excellent resemblance for the two samples, justifying the premise for their comparison in the present context.

The nanocrystal-film comparison presented in Figures 2 and 3 was augmented with TT measurements on $MAPbI_3$ prepared on NSF6 flint glass. Figure 4 presents TT data collected 3 ps after photoexcitation of this sample from either of its faces for two pump fluences. Again the similarity of both transient spectra is striking as demonstrated by the subtraction of the two, depicted in the blue curves. The main difference is a minor feature at the BE resembling a first derivative of the exciton band and a marginally larger amplitude for the broad reduced transmission in the case of irradiation through the flint glass. Accordingly, transferring the excited carriers from the air/LHP to the flint glass/LHP interface has only a small effect on differential transmission, including the 500−700 nm band of reduced transmission which is at the focus of this discussion.

Pump−probe measurements record photoinduced changes in transmission resulting from absorption throughout the sample and reflection off all refractive discontinuities.[31] For films whose thickness is near to the light wavelength, this may also be effected by interference of waves reflected off adjacent discontinuities. In our discussion this scenario will be simplified. Since we are only interested in *changes* in transmission, only surfaces where one index of refraction is significantly changing will be considered (*i.e.*, the face through which pump is applied in these optically thick films). Given the roughness of air/LHP surfaces, interference effects are neglected as well. The literature debate addressed here concerns the relative part played by reflectivity in the measured transmission changes and, as detailed in eq 2, involves both parts of the refractive index:

$$\frac{dR}{d\kappa} = \frac{8nn_0\kappa}{(n_0^2 + 2nn_0 + n^2 + \kappa^2)^2}; \frac{dR}{dn} = \frac{-4n_0(\kappa^2 + n_0^2 - n^2)}{(n_0^2 + 2nn_0 + n^2 + \kappa^2)^2} \quad (3)$$

We start by using eqs 2 and 3 to roughly estimate how strongly reflectivity changes should contribute to TT spectra in the perovskite thin films under study. Starting from the nanodot/film comparison, the relevant (dimensionless) first derivatives of R appear in the quartz/LHP row of Table 1. Whether referring to $\Delta\kappa$ or Δn, the derivative magnitudes range from 0.1 to 0.02. In order to compare differential reflection and absorption on equal footing, the latter needs to be considered for a defined thickness. Since the films are optically thick, the transmitted wave then experiences differential absorption effectively within the pump penetration depth $l \sim 100$ nm. In terms of absorption losses and using a linear approximation for differential sample absorption: $(e^{-\Delta\alpha l} \cong 1 - \Delta\alpha l)$, $\Delta\alpha l = 4\pi\Delta\kappa l/\lambda$ leading to a first derivative with respect to κ of: $\frac{d\Delta\alpha l}{d\kappa} = \frac{4\pi l}{\lambda}$. Substituting correct values for these constants, $d\Delta\alpha l/d\kappa \approx 2$, more than an order of magnitude larger than the derivatives in eq 3. Assuming photoinduced variations $\Delta\kappa$ and Δn of roughly similar magnitude, absorptive effects of $\Delta\kappa$ should accordingly dominate differential transmission in the thin films on quartz.

Similar expressions for nanocrystal $d\sigma/d\kappa$ and $d\sigma/dn$ are more intricate. As detailed in the Supporting Information, two main observations help to complete the comparison. First, $d\sigma/dn$ has a complex functional dependence on all three optical constants (n_0, n, κ), and its value throughout the probed spectral range is opposite to that of $d\sigma/d\kappa$ and roughly an order of magnitude smaller in absolute value. Second, given the relative values of constants n_0, n, and κ, $d\sigma/d\kappa$ is nearly constant reflecting a simple linear dependence of the cross section on the extinction throughout the probed range. Once these

DOI: 10.1021/acsnano.8b01570
ACS Nano 2018, 12, 5719−5725

observations concerning σ are factored in with the estimated influence of differential reflectivity in films, the striking similarity of TT data in both $CsPbI_3$ samples indicates that thin-film pump−probe data must be dominated by absorbance and can be interpreted nearly quantitatively as such.

The results presented in Figure 4 are compatible with the dominance of absorption changes in TT data for perovskite thin films. The initial profile of excitation density *vs* depth is exponential, and with a sample OD of 1 at the nominal pump wavelength, this density falls by 1 order of magnitude going from the entrance to exit face. As determined by Beard and coworkers,[28] timescales for the equilibration of such profiles in $MAPbI_3$ films of similar thickness show that it takes place on tens of ps, significantly longer than the 3 ps delay for the TT data presented in Figure 4. We can therefore assume that this exponential profile is maintained during the pump−probe delay. In accordance with the assumptions outlined above, the differential reflection in these experiments can be assigned to that experienced at the pump entrance face. But as demonstrated in Table 1, sensitivity of the air/LHP surface reflectivity to changes in index is significantly higher than for the NSF6/LHP surface, particularly for changes in n which in any case dominates reflectivity here. Thus the near equality of the TT data, probed always from the air/LHP surface, but excited from either face of the sample, again suggests that reflectivity changes play a minor role in determining difference transmission in LHP films.

We emphasize that the thin films and nanocrystals of $CsPbI_3$ perovskite were not exposed to air at any stage from preparation to pump−probe measurements. In the case of the $MAPbI_3$ samples, indeed the pump−probe measurements were conducted in ambient atmosphere, within one day after preparation. However, the samples do not show any indication of degradation to PbI_2 throughout the experiments. Therefore reported effects of humidity and substrate microstructure on later stages of carrier evolution are irrelevant to this study.[38−40]

This result is very important since numerous pump−probe experiments conducted on LHP films to date have been interpreted in terms of changes in sample absorbance, often without considering differential reflectance.[5,7,13−16,18,19,21,25,26] If indeed both contributions to TT were of similar magnitude, much of the analysis and many of the conclusions arrived at in that literature would be tainted, requiring radical reassessment. Luckily it appears that interpreting pump−probe data, assuming it stems from photoinduced alteration of absorbance alone, is essentially correct. This is not to say that all assignments of TT spectra in the literature are correct, but that they are based on a meaningful observable and that this simplified approach can be used in future keeping in mind that slight corrections are required for factoring in the weaker reflectivity changes. In light of all results reported above the 550−650 nm PIA is assigned to BG renormalization of the interband absorption.[18,20] Since this enhanced absorption overlaps with the evolving bleach due to state filling, it is gradually uncovered in the visible while hot carriers cool to the BE, producing the apparent rising in the net absorption amplitude.

CONCLUSIONS

The contested impact of reflectivity changes on transient transmission in lead halide perovskite films is addressed here by comparing data in photoexcited $CsPbI_3$ films with that obtained in large nanocrystals of the same material. This unconventional recourse to nanocrystal photophysics provides a test which does not rely on cross inferences between absorption and reflection measurements using complex mathematical manipulations. It relies on the very different dependence of nanodot absorption and thin-film reflectance on the materials index of refraction. Results prove reflectivity changes do not make a major contribution to transient transmission spectra as suggested in some earlier reports. None of the characteristic spectral signatures revealed in numerous pump−probe experiments are exclusively due to, or even strongly affected by, changes in sample reflectivity. This conclusion is strengthened by a related study of polycrystalline $MAPbI_3$ films formed on flint glass. Together, both experiments validate interpretation of pump−probe data in semitransparent perovskite films primarily in terms of sample absorbance, with reflectivity making only minor contributions to transmission changes.

MATERIALS AND METHODS

Preparation of $CsPbI_3$ Nanocrystals. Lead iodide (PbI_2, 99.9%), cesium carbonate (Cs_2CO_3, 99.9%), octadecene (ODE, Tech. 90%), oleic acid (OA, Tech. 90%), and oleylamine (OLA, Tech. 70%) were purchased from Sigma Aldrich. $CsPbI_3$ nanocrystals were synthesized according to a previously published procedure.[41] Briefly, 0.26 g of PbI_2 were dissolved in 15 mL ODE, 1.5 mL OA, and 1.5 mL OLA in a three-necked-flask and degassed at 120 °C. Next, 0.2 g of Cs_2CO_3 was dissolved in 7.5 mL ODE and 0.625 mL OA in a three-necked-flask and degassed at 120 °C. Then, under argon atmosphere, the lead iodide precursor solution was heated to 140 °C, and a hot syringe was used to swiftly inject 1.2 mL of the Cs precursor into the PbI_2 precursor solution, yielding a deep red colloid. The reaction was quenched with an ice bath, 10 s after the injection of the Cs precursor. Finally, the $CsPbI_3$ product was isolated directly from the ODE by centrifugation (6000 rpm for 10 min) and redispersed in hexane. The nanocrystals were characterized using transmission electron microscopy (TEM) and photoluminescence (PL) spectroscopy (Figures S1 and S2 in the Supporting Information).

Preparation of $CsPbI_3$ Thin Films. The solution of $CsPbI_3$ was prepared by dissolving an equimolar amount of PbI_2 and CsI (Sigma Aldrich) in dimethylformamide at a concertation of 0.48 mM.[42] The $CsPbI_3$ perovskite film fabrication was done on microscope glass in a nitrogen filled glovebox by one step deposition which composed of two stages: First, a spin of 10 s at 1000 rpm, followed by a 60 s spin at 5000 rpm. Slightly before the $CsPbI_3$ deposition 33 μL of HI (57 wt% in H_2O sigma) was added to the precursor solution, the films were annealed at 110 °C until becoming black. The $CsPbI_3$ films were encapsulated using an additional glass in order to prevent phase transformation of the $CsPbI_3$ perovskite to the yellow phase.

Preparation of $MAPbI_3$ Thin Films. Thin films of $MAPbI_3$ perovskites were prepared according to a previous published procedure.[43] Briefly, the first spin coating of 1 M solutions of PbI_2 in dimethylformamide was carried out on high-index glass (NSF6) substrates at a spin velocity of 6500 rpm for 5 s. After the spin-coating, the substrates were annealed at 80 °C for 10 min. In the next step, the spin-coated PbI_2 films were dipped into a solution of 63 mM methylammonium iodide (CH_3NH_3I) in isopropanol. In subsequent step, the samples were annealed at 80 °C for another 30 min. Figure S3 presents the photoluminescence spectrum of the films. Powder XRD pattern of the sample is shown in the Figure S4.

Details of the Pump−Probe Measurement. The pump−probe experiments were carried with home-built multipassed amplified Ti-Sapphire laser producing 30 fs pulses at 790 nm with 1 mJ of energy at 1 kHz repetition rate. The laser fundamental was split into two for generation of pump and probe pulses. The pump pulses were produced from non-collinear optical parametric amplifier (NOPA) centered at 520 nm. The pump pulses were compressed to 10% of their transform limit using a pair of chirp mirror (Venteon Optics, Laser Quantum). The supercontinuum probe pulses were generated by focusing 1300 nm output pulses of an optical parametric amplifier

DOI: 10.1021/acsnano.8b01570
ACS Nano 2018, 12, 5719−5725

(TOPAS 800, Light Conversion) on a 2 mm BaF_2 crystal. The white light probe pulses were also dispersion corrected using another pair of chirp mirrors before they were directed toward the sample using all reflective optics.

The first set of experiments was carried out to compare the results of pump−probe measurements between nanocrystals and thin films of $CsPbI_3$. The nanocrystals of $CsPbI_3$ in hexane were placed on a 1 mm quartz cell for the pump−probe study. The thin films of $CsPbI_3$ were prepared on a 0.5 mm glass substrate and encapsulated using another 0.1 mm thin glass. The pump and the probe beams were facing the 0.5 mm glass/$CsPbI_3$ side.

The aim of the second set of experiments was to compare the results by exciting $MAPbI_3$ thin films from different interfaces. The films of $MAPbI_3$ were prepared on a high-index glass (NSF6) substrate. The probe pulses were always sent from air/$MAPbI_3$ interface. The pump pulses were sent from either air/$MAPbI_3$ interface or NSF6/$MAPbI_3$ interface. The absorbance of the sample at the pump wavelength was adjusted to ∼1, such that most of the excited carriers are formed toward the front surface during the probing (Yang *et al.* ref 28). All the experiments were carried out with weak excitation pump fluence to avoid any multiphoton event.

ASSOCIATED CONTENT

Supporting Information

The Supporting Information is available free of charge on the ACS Publications website at DOI: 10.1021/acsnano.8b01570.

Equations for first derivatives of absorption cross-section of a nanocrystal with respect to n and κ, TEM images of the nanocrystals and PL spectra of thin films/nanocrystals (PDF)

AUTHOR INFORMATION

Corresponding Author

*E-mail: sandy@mail.huji.ac.il

ORCID

Tufan Ghosh: 0000-0002-4898-2117
Lioz Etgar: 0000-0001-6158-8520
Sanford Ruhman: 0000-0003-0575-1367

Notes

The authors declare no competing financial interest.

ACKNOWLEDGMENTS

S.R. holds the Lester Aronberg Chair in Chemistry. S.R. acknowledges support from the US-Israel Binational Science Foundation and the Israel Science Foundation. T.G. thanks the Lady Davis Fellowship Trust and the Raymond and Janine Bollag Post-Doctoral Fellowship Fund for a fellowship. S.R. and T.G. thank O. Liubashevski for technical support. L.E. would like to thank the Israel Ministry of Science for their financial support.

REFERENCES

(1) Kojima, A.; Teshima, K.; Shirai, Y.; Miyasaka, T. Organometal Halide Perovskites as Visible-Light Sensitizers for Photovoltaic Cells. *J. Am. Chem. Soc.* **2009**, *131*, 6050−6051.

(2) Kim, H.-S.; Lee, C.-R.; Im, J.-H.; Lee, K.-B.; Moehl, T.; Marchioro, A.; Moon, S.-J.; Humphry-Baker, R.; Yum, J.-H.; Moser, J. E.; Grätzel, M.; Park, N.-G. Lead Iodide Perovskite Sensitized All-Solid-State Submicron Thin Film Mesoscopic Solar Cell with Efficiency Exceeding 9%. *Sci. Rep.* **2012**, *2*, 591.

(3) Lee, M. M.; Teuscher, J.; Miyasaka, T.; Murakami, T. N.; Snaith, H. J. Efficient Hybrid Solar Cells Based on Meso-Superstructured Organometal Halide Perovskites. *Science* **2012**, *338*, 643−647.

(4) Stranks, S. D.; Eperon, G. E.; Grancini, G.; Menelaou, C.; Alcocer, M. J. P.; Leijtens, T.; Herz, L. M.; Petrozza, A.; Snaith, H. J. Electron-Hole Diffusion Lengths Exceeding 1 Micrometer in an Organometal Trihalide Perovskite Absorber. *Science* **2013**, *342*, 341−344.

(5) Xing, G.; Mathews, N.; Sun, S.; Lim, S. S.; Lam, Y. M.; Grätzel, M.; Mhaisalkar, S.; Sum, T. C. Long-Range Balanced Electron- and Hole-Transport Lengths in Organic-Inorganic $CH_3NH_3PbI_3$. *Science* **2013**, *342*, 344−347.

(6) Grätzel, M. The Light and Shade of Perovskite Solar Cells. *Nat. Mater.* **2014**, *13*, 838−842.

(7) Ponseca, C. S.; Savenije, T. J.; Abdellah, M.; Zheng, K.; Yartsev, A.; Pascher, T.; Harlang, T.; Chabera, P.; Pullerits, T.; Stepanov, A.; Wolf, J.-P.; Sundström, V. Organometal Halide Perovskite Solar Cell Materials Rationalized: Ultrafast Charge Generation, High and Microsecond-Long Balanced Mobilities, and Slow Recombination. *J. Am. Chem. Soc.* **2014**, *136*, 5189−5192.

(8) Srimath Kandada, A. R.; Petrozza, A. Photophysics of Hybrid Lead Halide Perovskites: The Role of Microstructure. *Acc. Chem. Res.* **2016**, *49*, 536−544.

(9) Brenner, T. M.; Egger, D. A.; Kronik, L.; Hodes, G.; Cahen, D. Hybrid Organic—inorganic Perovskites: Low-Cost Semiconductors with Intriguing Charge-Transport Properties. *Nat. Rev. Mater.* **2016**, *1*, 15007.

(10) Huang, J.; Yuan, Y.; Shao, Y.; Yan, Y. Understanding the Physical Properties of Hybrid Perovskites for Photovoltaic Applications. *Nat. Rev. Mater.* **2017**, *2*, 17042.

(11) Guo, Y.; Yaffe, O.; Paley, D. W.; Beecher, A. N.; Hull, T. D.; Szpak, G.; Owen, J. S.; Brus, L. E.; Pimenta, M. A. Interplay between Organic Cations and Inorganic Framework and Incommensurability in Hybrid Lead-Halide Perovskite $CH_3NH_3PbBr_3$. *Phys. Rev. Mater.* **2017**, *1*, 042401.

(12) Bonn, M.; Miyata, K.; Hendry, E.; Zhu, X.-Y. Role of Dielectric Drag in Polaron Mobility in Lead Halide Perovskites. *ACS Energy Lett.* **2017**, *2*, 2555−2562.

(13) Manser, J. S.; Kamat, P. V. Band Filling with Free Charge Carriers in Organometal Halide Perovskites. *Nat. Photonics* **2014**, *8*, 737−743.

(14) Marchioro, A.; Teuscher, J.; Friedrich, D.; Kunst, M.; van de Krol, R.; Moehl, T.; Grätzel, M.; Moser, J.-E. Unravelling the Mechanism of Photoinduced Charge Transfer Processes in Lead Iodide Perovskite Solar Cells. *Nat. Photonics* **2014**, *8*, 250−255.

(15) Trinh, M. T.; Wu, X.; Niesner, D.; Zhu, X.-Y. Many-Body Interactions in Photo-Excited Lead Iodide Perovskite. *J. Mater. Chem. A* **2015**, *3*, 9285−9290.

(16) Piatkowski, P.; Cohen, B.; Ramos, F. J.; Nunzio, M. D.; Khaja Nazeeruddin, M.; Grätzel, M.; Ahmad, S.; Douhal, A. Direct Monitoring of Ultrafast Electron and Hole Dynamics in Perovskite Solar Cells. *Phys. Chem. Chem. Phys.* **2015**, *17*, 14674−14684.

(17) Rehman, W.; Milot, R. L.; Eperon, G. E.; Wehrenfennig, C.; Boland, J. L.; Snaith, H. J.; Johnston, M. B.; Herz, L. M. Charge-Carrier Dynamics and Mobilities in Formamidinium Lead Mixed-Halide Perovskites. *Adv. Mater.* **2015**, *27*, 7938−7944.

(18) Sharma, V.; Aharon, S.; Gdor, I.; Yang, C.; Etgar, L.; Ruhman, S. New Insights into Exciton Binding and Relaxation from High Time Resolution Ultrafast Spectroscopy of $CH_3NH_3PbI_3$ and $CH_3NH_3PbBr_3$ Films. *J. Mater. Chem. A* **2016**, *4*, 3546−3553.

(19) Zhai, Y.; Sheng, C. X.; Zhang, C.; Vardeny, Z. V. Ultrafast Spectroscopy of Photoexcitations in Organometal Trihalide Perovskites. *Adv. Funct. Mater.* **2016**, *26*, 1617−1627.

(20) Yang, Y.; Ostrowski, D. P.; France, R. M.; Zhu, K.; van de Lagemaat, J.; Luther, J. M.; Beard, M. C. Observation of a Hot-Phonon Bottleneck in Lead-Iodide Perovskites. *Nat. Photonics* **2016**, *10*, 53−59.

(21) Bretschneider, S. A.; Laquai, F.; Bonn, M. Trap-Free Hot Carrier Relaxation in Lead−Halide Perovskite Films. *J. Phys. Chem. C* **2017**, *121*, 11201−11206.

DOI: 10.1021/acsnano.8b01570
ACS Nano 2018, 12, 5719−5725

(22) Wu, K.; Liang, G.; Shang, Q.; Ren, Y.; Kong, D.; Lian, T. Ultrafast Interfacial Electron and Hole Transfer from $CsPbBr_3$ Perovskite Quantum Dots. *J. Am. Chem. Soc.* **2015**, *137*, 12792−12795.
(23) Butkus, J.; Vashishtha, P.; Chen, K.; Gallaher, J. K.; Prasad, S. K. K.; Metin, D. Z.; Laufersky, G.; Gaston, N.; Halpert, J. E.; Hodgkiss, J. M. The Evolution of Quantum Confinement in $CsPbBr_3$ Perovskite Nanocrystals. *Chem. Mater.* **2017**, *29*, 3644−3652.
(24) Mondal, N.; Samanta, A. Complete Ultrafast Charge Carrier Dynamics in Photo-Excited All-Inorganic Perovskite Nanocrystals ($CsPbX_3$). *Nanoscale* **2017**, *9*, 1878−1885.
(25) Ghosh, T.; Aharon, S.; Etgar, L.; Ruhman, S. Free Carrier Emergence and Onset of Electron−Phonon Coupling in Methylammonium Lead Halide Perovskite Films. *J. Am. Chem. Soc.* **2017**, *139*, 18262−18270.
(26) Anand, B.; Sampat, S.; Danilov, E. O.; Peng, W.; Rupich, S. M.; Chabal, Y. J.; Gartstein, Y. N.; Malko, A. V. Broadband Transient Absorption Study of Photoexcitations in Lead Halide Perovskites: Towards a Multiband Picture. *Phys. Rev. B: Condens. Matter Mater. Phys.* **2016**, *93*, 161205.
(27) Price, M. B.; Butkus, J.; Jellicoe, T. C.; Sadhanala, A.; Briane, A.; Halpert, J. E.; Broch, K.; Hodgkiss, J. M.; Friend, R. H.; Deschler, F. Hot-Carrier Cooling and Photoinduced Refractive Index Changes in Organic−Inorganic Lead Halide Perovskites. *Nat. Commun.* **2015**, *6*, 8420.
(28) Yang, Y.; Yang, M.; Moore, D. T.; Yan, Y.; Miller, E. M.; Zhu, K.; Beard, M. C. Top and Bottom Surfaces Limit Carrier Lifetime in Lead Iodide Perovskite Films. *Nature Energy* **2017**, *2*, 16207.
(29) Green, M. A.; Jiang, Y.; Soufiani, A. M.; Ho-Baillie, A. Optical Properties of Photovoltaic Organic−Inorganic Lead Halide Perovskites. *J. Phys. Chem. Lett.* **2015**, *6*, 4774−4785.
(30) Leguy, A. M. A.; Azarhoosh, P.; Alonso, M. I.; Campoy-Quiles, M.; Weber, O. J.; Yao, J.; Bryant, D.; Weller, M. T.; Nelson, J.; Walsh, A.; van Schilfgaarde, M.; Barnes, P. R. F. Experimental and Theoretical Optical Properties of Methylammonium Lead Halide Perovskites. *Nanoscale* **2016**, *8*, 6317−6327.
(31) Shah, J. *Ultrafast Spectroscopy of Semiconductors and Semiconductor Nanostructures*; Springer Science & Business Media: New York, 2013.
(32) Leatherdale, C. A.; Woo, W.-K.; Mikulec, F. V.; Bawendi, M. G. On the Absorption Cross Section of CdSe Nanocrystal Quantum Dots. *J. Phys. Chem. B* **2002**, *106*, 7619−7622.
(33) Gosnell, J. D.; Weiss, S. M. Light Scattering by White-Emitting CdSe Nanocrystals and Traditional YAG: Ce^{3+} Phosphor Particles. *Mater. Res. Soc. Symp. Proc.* **2009**, *1148*, 1148-PP09-02.
(34) Brus, L. E. Electron−electron and Electron-hole Interactions in Small Semiconductor Crystallites: The Size Dependence of the Lowest Excited Electronic State. *J. Chem. Phys.* **1984**, *80*, 4403−4409.
(35) El-Sayed, M. A. Small Is Different: Shape-, Size-, and Composition-Dependent Properties of Some Colloidal Semiconductor Nanocrystals. *Acc. Chem. Res.* **2004**, *37*, 326−333.
(36) Protesescu, L.; Yakunin, S.; Bodnarchuk, M. I.; Krieg, F.; Caputo, R.; Hendon, C. H.; Yang, R. X.; Walsh, A.; Kovalenko, M. V. Nanocrystals of Cesium Lead Halide Perovskites ($CsPbX_3$, X = Cl, Br, and I): Novel Optoelectronic Materials Showing Bright Emission with Wide Color Gamut. *Nano Lett.* **2015**, *15*, 3692−3696.
(37) Berdiyorov, G. R.; Kachmar, A.; El-Mellouhi, F.; Carignano, M. A.; El-Amine Madjet, M. Role of Cations on the Electronic Transport and Optical Properties of Lead-Iodide Perovskites. *J. Phys. Chem. C* **2016**, *120*, 16259−16270.
(38) Leguy, A. M. A.; Hu, Y.; Campoy-Quiles, M.; Alonso, M. I.; Weber, O. J.; Azarhoosh, P.; van Schilfgaarde, M.; Weller, M. T.; Bein, T.; Nelson, J.; Docampo, P.; Barnes, P. R. F. Reversible Hydration of $CH_3NH_3PbI_3$ in Films, Single Crystals, and Solar Cells. *Chem. Mater.* **2015**, *27*, 3397−3407.
(39) Serpetzoglou, E.; Konidakis, I.; Kakavelakis, G.; Maksudov, T.; Kymakis, E.; Stratakis, E. Improved Carrier Transport in Perovskite Solar Cells Probed by Femtosecond Transient Absorption Spectroscopy. *ACS Appl. Mater. Interfaces* **2017**, *9*, 43910−43919.
(40) Bi, C.; Wang, Q.; Shao, Y.; Yuan, Y.; Xiao, Z.; Huang, J. Non-Wetting Surface-Driven High-Aspect-Ratio Crystalline Grain Growth for Efficient Hybrid Perovskite Solar Cells. *Nat. Commun.* **2015**, *6*, 7747.
(41) Koolyk, M.; Amgar, D.; Aharon, S.; Etgar, L. Kinetics of Cesium Lead Halide Perovskite Nanoparticle Growth; Focusing and de-Focusing of Size Distribution. *Nanoscale* **2016**, *8*, 6403−6409.
(42) Eperon, G. E.; Paternò, G. M.; Sutton, R. J.; Zampetti, A.; Haghighirad, A. A.; Cacialli, F.; Snaith, H. J. Inorganic Caesium Lead Iodide Perovskite Solar Cells. *J. Mater. Chem. A* **2015**, *3*, 19688−19695.
(43) Aharon, S.; Cohen, B. E.; Etgar, L. Hybrid Lead Halide Iodide and Lead Halide Bromide in Efficient Hole Conductor Free Perovskite Solar Cell. *J. Phys. Chem. C* **2014**, *118*, 17160−17165.

DOI: 10.1021/acsnano.8b01570
ACS Nano 2018, 12, 5719−5725